Low-loss electron beam transport in a high-power, electrostatic free-electron maser

Nuclear Instruments and Methods in Physics Research A 390 (1997) 409–416

NUCLEAR INSTRUMENTS & METHODS IN PHYSICS RESEARCH Section A

ELSEVIER

Low-loss electron beam transport in a high-power, electrostatic free-electron maser

M. Valentini, C.A.J. van der Geer, A.G.A. Verhoeven, M.J. van der Wiel, W.H. Urbanus*, and the FEM team

FOM Instituut voor Plasmafysica Rijnhuizen, Association EURATOM-FOM, Postbus 1207, 3430 BE Nieuwegein, Netherlands

Received 24 February 1997

Abstract

At the FOM Institute for Plasma Physics "Rijnhuizen", The Netherlands, the commissioning of a high-power, electrostatic free-electron maser is in progress. The design target is the generation of 1 MW microwave power in the frequency range 130–260 GHz. The foreseen application of this kind of device is as a power source for electron cyclotron applications on magnetically confined plasmas.

The device is driven by a high-power electron beam. For long-pulse operation a low loss current is essential. A 3-A electron beam has been accelerated to energies ranging from 1.35 to 1.7 MeV and transported through the undulator at current losses below 0.02%. Further, it was shown that the beam line accepts an electron energy variation of 5% with fixed beam optics. This is essential for rapid tuning of the microwave frequency, over 10%.

Electron beam simulations have shown to be remarkably accurate both for the prediction of the lens settings and for the intercepted current. The operational settings of the beam line which give the highest current transmission are within a few percent of the simulated values.

PACS: 41.75.H; 41.60.C; 29.17

1. Introduction

The principal aim of present Free-Electron Maser (FEM) research is the realisation of a source of microwave radiation of high average power, high system efficiency, and broad tunability [1]. The achievement of these targets may culminate in the use of FEMs as power sources for electron cyclotron applications on magnetically confined plasmas in future fusion research devices, such as ITER. For such applications power sources of at least 1 MW of microwave power in the frequency range 140–200 GHz at a system efficiency of 50% are required [2]. Fast tunability (on ms scale) in a frequency range of a few percent would be an advantage.

FEMs combine the advantages of present high-power, high-frequency, microwave sources, such as gyrotrons, with the additional advantages of continuous tunability over a large range, higher frequency, and eventually a higher power per unit.

In a FEM radiation is generated by a relativistic electron beam oscillating in an undulator. The achievement of the above-mentioned targets largely depends on the accelerator technology used to generate the driving beam. A promising approach involves the use of the electrostatic acceleration technology with electron beam energy recovery. In this scheme the electron beam is accelerated to the interaction region, i.e. the undulator, and afterwards it is decelerated and collected in a multistage depressed collector. On deceleration, the electron beam transfers back part of its energy to the dc accelerator voltage supply, thus limiting the required power. In order to limit the electron beam power, an extraction efficiency, i.e., the fraction of the electron beam power which is transferred to the microwaves, of the order of a few percent is required. A higher extraction efficiency is not useful because it causes a too large energy spread after the FEL interaction, complicating beam transport through the energy recovery section.

The electron beam power after deceleration is of the order of the generated microwave power. Thus, a multistage depressed collector is needed to optimise the system

*Corresponding author. Tel.: + 31 30 6096999; fax: + 31 30 6031204; e-mail: urbanus@rijnh.nl.

PII S0168-9002(97)00478-6

efficiency [3]. The main beam power is supplied at the collector side, after beam deceleration, at a potential level as close as possible to ground potential, while the accelerator voltage generator has to supply only the beam loss current. Full CW operation is subject to the achievement of a very high degree of beam transmission through the beam line and of beam recovery in a depressed collector.

A high power, electrostatic FEM is under construction at the FOM Institute for Plasma Physics Rijnhuizen, The Netherlands [4,5]. The principal design parameters of the Fusion FEM are presented in Table 1. The design target is the generation of 1 MW microwave power, tuneable in the frequency range from 130 to 260 GHz, at a system efficiency of over 50%. The frequency range is covered by changing the electron beam energy from 1.35 to 2.0 MeV. Since high dc voltages are used, the system is placed in a pressure vessel filled with SF_6. A dc, 80 kV, 12 A, triode electron gun generates the driving electron beam.

The Fusion FEM experiment involves several challenges:

- low-loss ($< 0.2\%$) electron beam transmission,
- generation of high power microwaves in a broad frequency range,
- fast tunability (on ms scale) in a frequency range of $\Delta\nu \approx 10\%$. This requires a beam line acceptance in terms of beam energy variation of a few percent ($\Delta E \approx 5\%$) with fixed beam optics.
- a high degree of electron beam (current and power) recovery in a multistage depressed collector,

In this paper we present the results of electron beam transmission experiments through the beam line of the Fusion FEM. The electron beam is transmitted with negligible losses (0.02%). The electron beam transport simulations have shown to be remarkably reliable both for the prediction of the operational settings of the beam line and the intercepted current. The operational settings of the beam line which give the highest current transmission are within a few percent of the simulated values.

Table 1
Principal design parameters of the Fusion FEM

Gun voltage	80 kV
Electron beam current	12 A
Rms xx' emittance	$\leq 10\pi$ mm mrad
Electron beam energy	1.35–2 MeV
Pulse length (final stage)	100 ms
Pulse length (Phase I)	10 μs
Microwave frequency	130–260 GHz
Microwave net power	1 MW
Target system efficiency	$\geq 50\%$
Target current losses	≤ 20 mA
Linear gain per pass	7–10
Gain at saturation	3.5
Waveguide dimension	15×20 mm^2
Waveguide mode	HE_{11}
Type of reflector	Stepped waveguide
Undulator period	40 mm
Number of undulator periods, section 1	20
Number of undulator periods, section 2	14
Undulator field, section 1	0.2 T
Undulator field, section 2	0.16 T

2. The design of the electron beam line

The Fusion FEM is presently being constructed and tested in an inverse set-up to verify the beam transport characteristics and microwave output (see Fig. 1). The electron gun is mounted inside the high-voltage terminal, and the undulator and microwave cavity are outside the pressure tank. In terms of electron beam transport, this configuration is equivalent to the nominal one, with the exception that no decelerator and recovery system are mounted. In this set-up the electron beam is supplied by the capacitance of the high-voltage terminal (1 nF) and the pulse length is limited by the accelerator voltage drop.

Important features of the beam line design which are incorporated to ensure low interception current and low emittance growth, of the order of 15%, are: a straight beam line, an emittance-conserving solenoid focusing system, and a large phase-space acceptance ($\approx 60\pi$ mm mrad, rms xx'-value). The beam halo current is suppressed at the cathode by using an edge emission suppression ring [6]. In addition, the electron gun is equipped with a focus electrode, mounted around the cathode, to enable control of the beam quality directly from the cathode. As a result a top-hat profile, low emittance ($\leq 10\pi$ mm mrad, rms xx'-value) electron beam is generated.

The microwave cavity consists of a waveguide inside the undulator and so-called stepped waveguides are located upstream and downstream of the undulator. In the stepped waveguides the microwave beam is split into two identical off-axis beams, so as to separate the microwaves from the electron beam. At the position of full separation mirrors are mounted to reflect the microwave beams back into the undulator. The upstream mirrors provide 100% reflection, while the downstream mirrors can be adjusted to tune the reflection coefficient [5]. The cross section of the microwave cavity is 15×20 mm^2 in the undulator waveguide and 50×20 mm^2 in the stepped waveguides.

The electron beam transport and focusing system consists of air-core and iron-core solenoids; see Fig. 1. Large-dimension air-core solenoids are used where low fields are needed and where the beam has a large diameter, in order to have a low filling factor. Iron-core lenses are used to generate the required high field to focus the beam into the microwave cavity and to match the beam to the undulator acceptance.

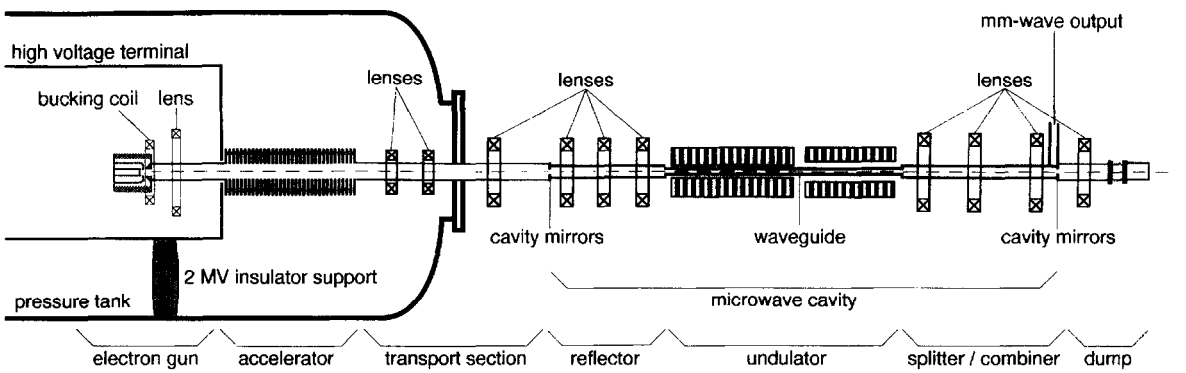

Fig. 1. Layout of the Fusion FEM in the inverse set-up.

An air-core solenoid matches the beam from the gun to the accelerator. Great care is taken to minimise the flux from the focusing system leaking on the cathode. A bucking coil is placed next to the gun and cancels the tail magnetic field and its first derivative on the cathode surface. Two air-core solenoids transport the beam from the accelerator to the microwave cavity. An iron-core solenoid focuses the beam in the microwave cavity and three iron-core solenoids arranged in a periodic focusing system transport the beam through the feedback system of the microwave cavity and match it to the acceptance of the undulator periodic focusing scheme.

The required high current transmission imposes the beam to be continuously focused. Inside the undulator this is achieved by using a planar undulator equipped with side arrays of permanent magnets [7]. This configuration provides both field enhancement and focusing in the wiggle and non-wiggle plane. The undulator is tuned to provide equal focusing in both planes. This way, the electron beam cylindrical symmetry is almost preserved. The generation of microwave power is optimized by step-tapering the undulator field. The undulator consists of two sections of constant field. The undulator field (2.0 kG in the first section, and 1.6 kG in the second), and number of periods (20 in the first section and 14 in the second) are chosen to reach the required high gain per pass of the radiation field and the target extraction efficiency of around 6% [8,9].

Since during this experimental phase interest is focused on low-loss electron beam transmission through the undulator waveguide, which is the part of the beam line with the lowest acceptance, the beam line ends behind the undulator in a simple dump (see Fig. 2).

The position of the electron beam diagnostics is shown in Fig. 2. The beam current emitted from the cathode and the current in the dump are measured. To determine the beam losses with sufficient accuracy, the intercepted currents are measured directly at critical places of the beam line: on apertures located behind the accelerator and in

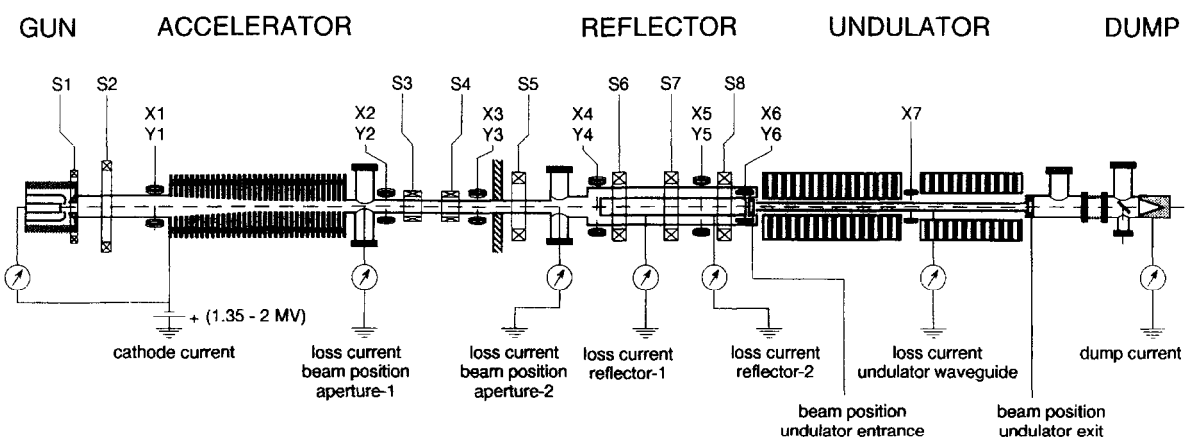

Fig. 2. Electron beam diagnostics used in the present experiments.

front of the reflector, on the reflector waveguide walls, and on the undulator waveguide walls.

The position of the beam centre of charge is reconstructed by measuring the induced charge on pick-up electrodes arranged about the beam line axis, inside the vacuum pipe. These beam position monitors are located just behind the accelerator tube, in front of the mirrors of the microwave cavity, and at the entrance and exit of the undulator.

3. Simulation of the electron beam dynamics

The design of the electron beam line is based on simulations performed using the 3-D particle-tracking code GPT [10] and a relativistic version of the Herrmann optical theory of thermal effects in electron beams [11, 12]. The GPT code follows the distribution of a number of macro-particles in real space and velocity space through the entire beam line. The effect of the various optical elements, lens misalignment, stray magnetic fields and steering coils can be accurately taken into account.

The Herrmann theory calculates current distribution functions semi-analytically everywhere along the beam line, allowing the determination of beam envelopes containing up to 99.9% of the beam current. Basically, the theory describes beam transport in terms of a superposition of the trajectories of electrons without thermal velocities emitted from the edge of the cathode, and of electrons with thermal velocities emitted from the cathode centre. The various trajectories are coupled via space charge. An initial uniform distribution in real space and a gaussian distribution in velocity space is assumed. This is consistent with actual gun characterisation measurements [6]. One of the main predictions of the Herrmann theory is that the current distribution evolves along the beam line from a uniform distribution to a Gaussian distribution and back to a uniform distribution at the focal planes. At these planes the initial uniform beam current profile at the cathode is imaged and thus no halo current is expected.

The simulation of the optimum position and operational parameters of the beam line components is an iterative procedure, which involves the use of the two codes during several steps. An initial set of parameters is calculated using the particle tracking code GPT. Then the Herrmann theory is used to optimise the beam line settings for 99.9% of the beam current. Particle simulations are performed again, with the modified settings. Iterations between the two codes are necessary to combine the advantages of the two approaches while minimising the influence of the respective approximations. In particular, the Herrmann theory assumes paraxial propagation of the electron beam and conservation of the beam emittance. In addition, the space-charge force is calculated using an ad hoc electron beam radius (i.e. the Herrmann radius). On the other hand, particle tracking codes have statistical difficulties in simulating the halo of the beam.

4. Electron beam transmission through the undulator

In Table 2 the design target and experimental performance of the electron beam transport system are summarised. The beam current was limited to 3 A. In order to operate in the space-charge-limited regime, the anode voltage was set at 35 kV. This way, the electron beam dynamics were self-similar to those of a 12 A, 80 kV beam. The electrostatic accelerator was operated at voltages ranging from 1.35 to 1.70 MV.

The measurements shown in Figs. 3–6 are for an electron energy of 1.55 MeV. As a first test, the current emitted from the cathode and the current collected in the dump are measured, see Figs. 3(a) and (b), respectively. The agreement between these measurements is within 1%, i.e., 30 mA.

The intercepted current is measured directly on apertures and waveguide sections, with an accuracy of ≤ 0.5 mA. In Fig. 4 the intercepted current on the two apertures at the accelerator exit (aperture 1, Fig. 4(a) and at the reflector entrance (aperture 2, Fig. 4(b) is shown. The line corresponding to the target value of 0.2% loss (i.e. 6 mA in the present case) is indicated. The current intercepted on apertures 1 and 2 is 1.5 and 0.5 mA, respectively. The diameter of these apertures was chosen slightly larger than the envelope of the 3 A beam, as to benchmark simulation codes against the actual beam envelope. The diameter of these apertures is not relevant for proper FEM operation and can be increased to eliminate the current losses shown in Fig. 4.

The peaks at the beginning and end of the electron pulse occur during the switch-on and switch-off times of the gun, when the gate electrode of the triode gun is switched from -12 kV (beam off) to 4.4 kV (beam on).

Table 2
Design targets and experimental performance of the Fusion FEM beam line in terms of electron beam transport.

	Design target	Experimental performance
Beam current	12 A	3 A
Gun voltage	80 kV	35 kV
Beam energy	1.35–2.0 MeV	1.35–1.70 MeV
Pulse length	10 μs	20 μs
Current losses	0.2%	0.02 %
Energy tunability with fixed beam optics	$\Delta E \approx 5\%$	$\Delta E \approx 5\%$

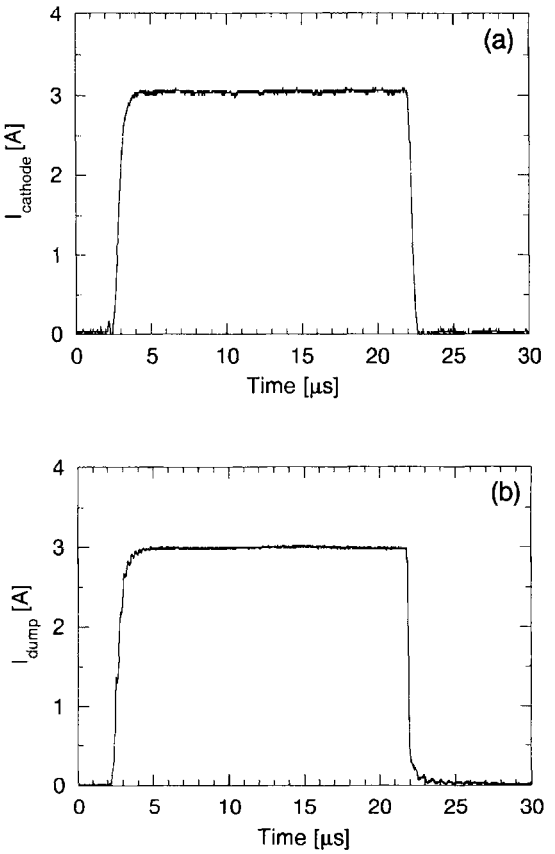

Fig. 3. (a) Current emitted from the cathode, and (b) current collected in the beam dump.

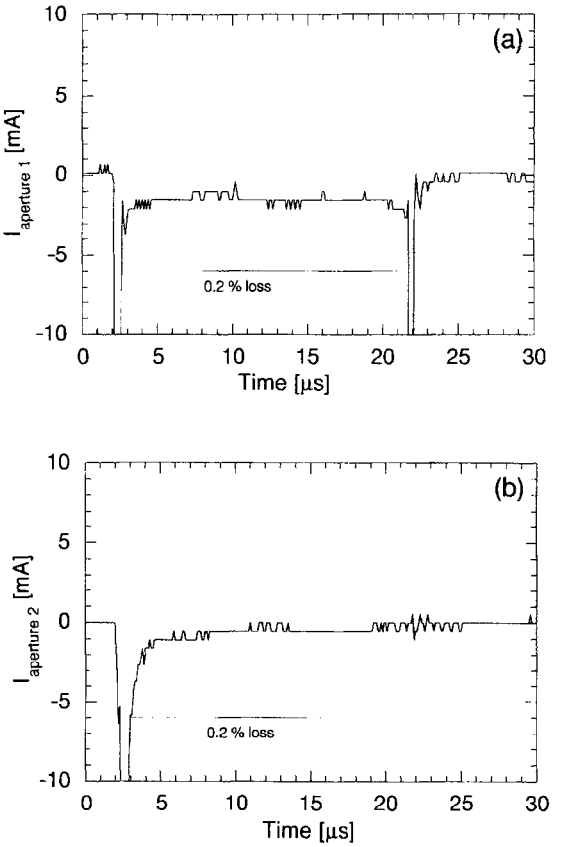

Fig. 4 (a) Current losses on the aperture behind the accelerator, and (b) in front of the reflector.

During the switch time ($\approx$ 150 ns), the electron beam is strongly divergent because the gun optics are not correct, and higher beam losses occur. The amplitude of these peaks showed to be highly sensitive to the beam position in the apertures and in the waveguides. The peaks, which are in fact undesired, were used as a very effective tool for beam alignment. Note that these short peaks will not affect the generation of microwave power.

The crucial part of the electron beam transmission experiment concerns the loss current in the waveguide structure. In Fig. 5 the intercepted current on the microwave cavity is shown. Apart from the switch-on and switch-off times of the gun, the intercepted current on the individual components (reflector walls, Fig. 5(a) and waveguide walls, Fig. 5(b) is hardly distinguishable from the digital noise level ($\leq$ 0.5 mA) of the diagnostics. The total loss current on these components is of the order of 0.5 mA. Regarding the intercepted current in the reflector and in the waveguide (Figs. 5(a) and 5(b), the peaks at the leading and trailing edge are produced by a combination of both beam losses and charges induced on the waveguide walls during the switch times of the gun. The two signals have the same sign during the switch-on time of the gun, while during the switch-off time the signals of the induced charges reverses sign, and the peak at the trailing edge is almost cancelled.

For beam energies of 1.35, 1.55, 1.63, and 1.70 MeV the same low loss currents have been reached. Note that in the dc acceleration system there are no restrictions to the choice of the electron beam energy.

Since fast-frequency tuning over 10% is required, the beam line must accept 5% energy variation with fixed lens settings. This was demonstrated by changing the electron beam energy by 5% (around 1.55 MeV). Beam transmission of 99.98% is possible in 10 μs pulses. The current losses during energy tunability in a larger range, or during longer pulses are concentrated at the beginning and end of the pulse. In Fig. 6 an example of current losses during 10% energy variation is shown.

5. Comparison between simulations and experiment

The simulated electron beam dynamics have been found to be in good agreement with the experimental

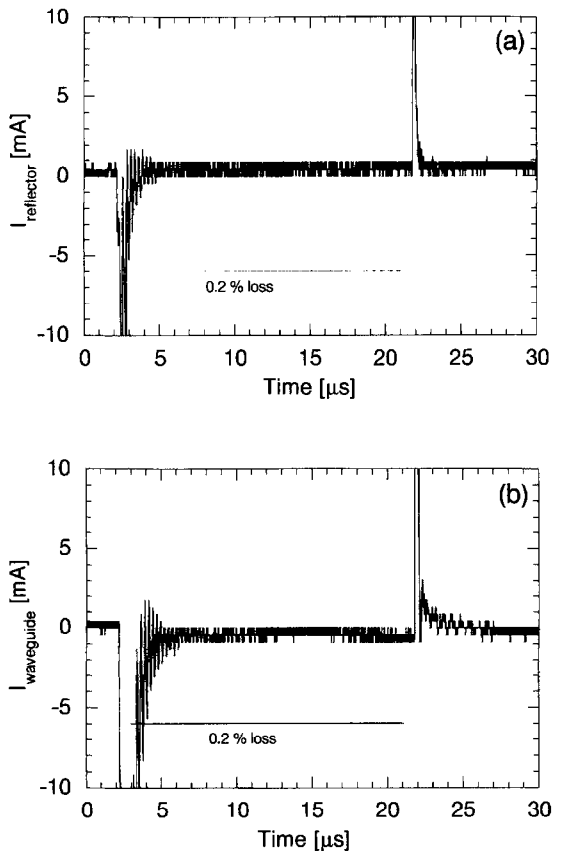

Fig. 5 Current losses in the microwave cavity components: (a) on the reflector walls, and (b) on the waveguide walls (inside the undulator).

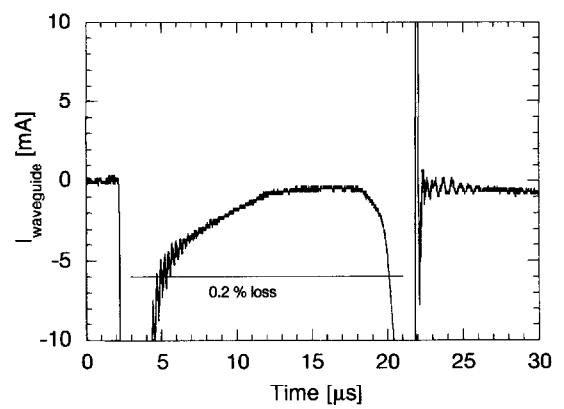

Fig. 6 Current losses in the undulator waveguide during 10% electron energy tuning with fixed beam optics.

results. In Table 3, a comparison between the simulated settings of the beam line and the settings which provide maximum current transmission in 20 μs pulses are shown. The discrepancy is of the order of a few percent.

Table 3
Lens and steering coil settings. The experimental settings are those which gave optimum transmission of the 3 A, 1.55 MeV, 20 μs electron pulse through the waveguide of the undulator

Beam line element	Simulated setting	Experimental setting
Lens 1	16.8 G	16.8 G
Lens 2	76.7 G	76.7 G
Steering coil		
set $x1$, $y1$	0/0 G cm	6/27 G cm
Seering coil		
set $x2$, $y2$	0/0 G cm	−13/ −3.6 G cm
Lens 3	170 G	170 G
Lens 4	170 G	170 G
Steering coil		
set $x3/y3$	0/0 G cm	−27/11 G cm
Lens 5	549 G	521 G
Steering coil		
set $x4/y4$	0/0 G cm	−17.4/6.9 Gcm
Lens 6	1136 G	994 G
Steering coil		
set $x5/y5$	0/0 G cm	3/0 G cm
Lens S7	700 G	693 G
Lens S8	1281 G	1313 G
Steering coil		
set $x6/y6$	0/0 G cm	0/0.6 Gcm

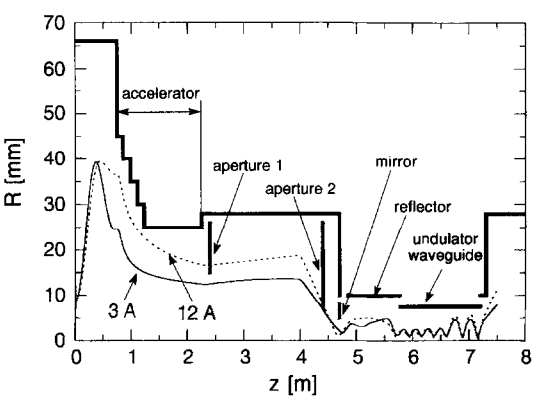

Fig. 7 Simulated envelope of 99.9% of the beam current. The solid and dashed curves are 3 A, 35 keV and 12 A, 80 keV. beams emerging from the gun, respectively. The final beam energy is 1.55 MeV. Also shown are the locations at which the intercepted current is measured.

Only lens 6, the one just behind the entrance of the microwave cavity (see Fig. 1), is an exception; the discrepancy between simulation and experiment is 12%. The fact that the experimental setting is lower than simulated indicates that the beam space charge force is lower than expected. Apparently, the beam radius is larger at lens 6, because the waist near the reflector entrance occurs before the reflector mirrors (compare the 3-A line in Fig. 7).

Since lens 4 is an air-core lens, the steel tank wall probably distorts the field of this lens, so that, only in the area between lens 4 and lens 6 (see Fig. 2), the beam envelope differs slightly from the simulations.

The loss current (1.5 mA) on the first aperture (see Fig. 4) is due to the halo of the beam. The intercepted current is consistent with both the expected percentage of halo current from the gun (0.1% i.e. 3 mA) and the prediction of the beam envelope at 99.9% of the total current shown in Fig. 7, i.e. the 3-A line. In addition, simulations based on the Herrmann theory show that the beam current profile at the accelerator exit is Gaussian, i.e. the halo current, composed by electrons having high transverse velocities, is far outside the computed beam envelope.

In Fig. 6 an example of current losses in the undulator waveguide for non-optimum settings of the beam line is shown. Although the intercepted current is higher than that shown in Fig. 5(b), it exceeds the target value of 0.2% only at the beginning and end of the pulse. This shows that these losses are due to the energy variation of the beam during the 20 μs pulse (60 keV) and are not produced by the halo of the beam. This is consistent with simulations based on the Herrmann theory, which predict that at injection into the undulator the uniform cathode current distribution is imaged and the halo current is focused back inside the beam envelope.

6. Significant results for operation at the designed specifications

Initial beam transport experiments have demonstrated low-loss transmission of a 3 A electron beam. The proven reliability of the electron beam simulations for the 3 A case validates the simulations for operation at the nominal current.

According to the Child–Langmuir law, at free expansion from the gun to the accelerator the dynamics of the 3 A, 35 keV electron beam are self-similar to that of the nominal 12 A, 80 keV beam. With an ad hoc setting of the lenses, the 12 A, 80 keV and the 3 A, 35 keV beam have the same radius at injection into the accelerator.

In Fig. 7, the simulated beam envelope at 99.9% of the total current is shown for the 3 A, 35 keV and the 12 A, 80 keV electron beam. The final beam energy is 1.55 MeV. The main difference between the two cases is the injection and transport inside the accelerator tube. Due to the higher space charge forces, the 12 A beam has a larger radius. This causes a larger beam radius behind the accelerator. However, with proper adjustment of the lens settings, the dimensions of the 12 A beam inside the reflector and the undulator waveguide are comparable to that of the 3 A beam. The simulations of Fig. 7 show that injection into the accelerator is the most critical part of the beam line. Due to the large beam radius, transport is very sensitive to the beam line settings.

The electrostatic accelerator system has been operated in the energy range 1.35–1.70 MeV. Operation in the range from 1.70 to 2.0 MeV is not expected to be more difficult in terms of beam transport, due to stronger focusing of the accelerator and lower space-charge forces.

7. Conclusion

Initial experiments on electron beam transport through the Fusion FEM beam line show that low-loss transmission is possible. The target loss-current in the Fusion FEM transport system is 20 mA at 12 A beam current, corresponding to 99.8% transmission. In the reported experiments a transmission from gun to beam dump of 99.95% has been achieved, at 3 A beam current. The current intercepted in the waveguide of the undulator, which is the part of the beam transport system with the smallest acceptance, is of the order of 0.5 mA, i.e., 0.02%.

The results at 3 A beam current are directly significant for operation at the nominal current of 12 A, for the following reasons. Firstly, the electron gun has been operated in the fully space-charge-limited regime at a reduced anode voltage, giving the same perveance and therefore self-similar behaviour to the nominal 12 A beam. Second, the simulation codes used to design the beam line and to predict sets of operational parameters are in very good agreement with the experimental results both for the prediction of the correct lens settings and the intercepted current.

The electrostatic accelerator system has been operated in the energy range 1.35–1.70 MeV. During microwave generation this would correspond to microwave frequencies in the range from 130 to 190 GHz. The electron beam energy can be tuned over 5% with fixed beam optics. During microwave generation, this would correspond to the target fast-tunability of 10% in frequency.

8. Acknowledgements

This work was performed as part of the research programme of the association agreement of EURATOM and the "Stichting voor Fundamenteel Onderzoek der Materie" (FOM) with financial support of the 'Nederlandse Organisatie voor Wetenschappelijk Onderzoek' (NWO) and EURATOM. One of the authors (M.V.) is supported by the Commission of the European Communities, Fusion Programme, contracts 5000-CT-94-5001, and 5004-CT-96-5016. The authors gratefully thank the High Voltage and ECH group of the Technical University of Eindhoven, who has resolved complicated problems in the field of electromagnetic compatibility.

9. References

[1] H. P. Freund, V. L. Granatstein, Nucl. Instr. and Meth. A 375 (1996) 665.
[2] M. Makowsky, in: M. von Ortenberg, H.U. Mueller (Eds.), Proc. 21st Int. Conf. on Infrared and Millimeter Waves, ISBN 3-00-000800-4, 1996, p. AW1.
[3] G. Ramian, Nucl. Instr. and Meth. A 318 (1992) 225.
[4] W. H. Urbanus et al., Nucl. Instr. and Meth. A 331 (1993) 235.
[5] W. H. Urbanus et al., Nucl. Instr. and Meth. A 358 (1995) 355.
[6] M. Cattelino, J. Atkinson, Varian Associates Interim Report, Palo Alto, January 1994.
[7] A. A. Varfolomeev et al., Nucl. Instr. and Meth. A 341 (1994) 462.
[8] M. Caplan, R.W.B. Best, A.G.A. Verhoeven, M.J. van der Wiel, W.H. Urbanus, V.L. Bratman, G.G. Denisov, Nucl. Instr. and Meth. A 331 (1993) 243.
[9] P. J. Eecen, T. J. Schep, A.V. Tulupov, Phys. Rev. E 52 (1995) 5460.
[10] S. B. van der Geer, M. J. de Loos, GPT Manual, Pulsar Physics, Utrecht, 1996.
[11] G. Herrmann, J. Appl. Phys. 29 (1958) 127.
[12] M. Caplan, M. Valentini, C. A. J. van der Geer, W. H. Urbanus, Nucl. Instr. and Meth. A 375 (1996) 91.